

High T_c superconductivity at the FeSe/SrTiO₃ Interface

Fa Wang,¹ Yuan-Yuan Xiang,² Da Wang,² Qiang-Hua Wang,² and Dung-Hai Lee^{3,4}

¹*Department of Physics, Massachusetts Institute of Technology,*

Cambridge, Massachusetts 02139, USA

²*National Lab of Solid State Microstructures,*

Nanjing University, Nanjing, 210093, China

³*Department of Physics, University of California*

at Berkeley, Berkeley, California 94720, USA

⁴*Materials Sciences Division, Lawrence Berkeley*

National Laboratory, Berkeley, California 94720, USA

(Dated: October 24, 2018)

Abstract

In a recent experiment the superconducting gap of a single unit cell thick FeSe film on SrTiO₃ substrate is observed by scanning tunneling spectroscopy and angle-resolved photoemission spectroscopy. The value of the superconducting gap is much larger than that of the bulk FeSe under ambient pressure. In this paper we study the effects of screening due to the ferroelectric phonons on Cooper pairing. We conclude it can significantly enhance the energy scale of Cooper pairing and even change the pairing symmetry. Our results also raise some concerns on whether phonons can be completely ignored for bulk iron-based superconductors.

I. INTRODUCTION

In a recent experiment[1] a single unit cell thick FeSe film is grown on the TiO_2 terminated (001) surface of SrTiO_3 (STO) by molecular beam epitaxy. Two gaps (~ 10 meV and 20 meV) are observed by scanning tunneling microscopy (STM) at low temperatures. At present there is no transport data and T_c is not determined. Subsequently an angle-resolved photoemission spectroscopy (ARPES) result appears.[2] According to this report, there is only electron Fermi surface, suggesting FeSe is electron doped. The observed electron pockets are nearly circular, and an approximately constant (~ 15 meV) superconducting gap is detected on them. Significantly, by studying the temperature dependence of the energy gap, an estimate of T_c , namely, 55 ± 5 K, is obtained. Currently there is no explanation of the two gap versus one gap discrepancy between the two measurements.

There are many unanswered questions. For examples, (1) What caused the FeSe doping? (2) Can the discrepancy between Ref.[1] and Ref.[2] be due to surface doping caused by the sample treatment prior to the ARPES measurement? (3) Are there buried, hence not yet detected, interface metallic bands?[2] (4) Are there interface ferroelectric ordering? (5) How strong is the coupling between the electrons in FeSe and the ferroelectric (FE) phonons in STO? Due to the uncertainty of the surface doping we shall study both undoped and electron doped FeSe.

STO is a “quantum paraelectric” insulator. The huge dielectric constant at low temperatures is due to the ionic movements. The associated phonon, the FE phonon, involve the relative displacement of the Ti and O atoms. An example of such displacement is shown in the right panel of Fig. 1. This phonon mode is soft at the zone center. At low temperatures bulk STO also undergoes an antiferrodistortive (AFD) transition. This distortion involves alternating clockwise and counterclockwise rotation of oxygens about titanium (see the left panel of Fig. 1) In a recent local density functional study[3] it is found, aside from zone folding, even static AFD distortion has little effect on the bandstructure. Therefore we shall ignore the AFD phonon in the following discussions.

In the rest of the paper we perform a two-stage renormalization group (RG) study.[4, 5] The first stage is a functional renormalization group (FRG)[6, 7] calculation. It determines the most important electronic scattering processes at low energies. As found in previous studies[7–9] for energies lower than the magnetic fluctuation energy scale, Λ_e , the strongest

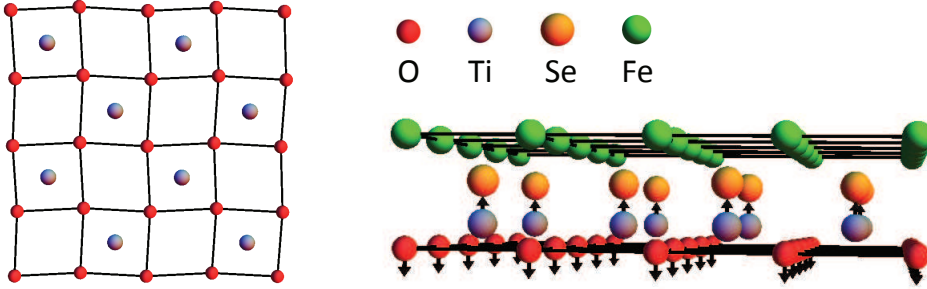


FIG. 1: Left panel: an example of AFD distortion in the TiO_2 plane. Right panel: a caricature of the frozen FE phonon with the atomic displacement in the (001) direction.

electron-electron scattering is in the Cooper channel (for superconducting samples). This is used as the input for the the second stage analysis. Here we study the effect of FE phonons at energies lower than the maximum phonon frequency $\Lambda_{ph} < \Lambda_e$. This is done by solving a generalized Eliashberg equation. The FE phonons have two important effects on the FeSe electrons. The first is to mix states separated by momentum (π, π) in the unfolded Brillouin zone. This is because a frozen FE phonon breaks the $z \leftrightarrow -z$ reflection symmetry, the symmetry that enables the Brillouin zone unfolding. In addition, the soft zone center FE phonons can screen the intra-pocket electron-electron repulsion.

II. THE MAIN RESULTS

To present the underlying physics, let's simplify the electronic structure by retaining only two Fermi pockets: the hole and electron pockets for the undoped FeSe/STO, and the two electron pockets for the doped FeSe/STO. The two main effects of FE phonon discussed earlier is described by an intra-pocket and an inter-pocket coupling constant, λ_{intra} and λ_{inter} . The superconducting transition temperature determined from the two-stage RG approach

is given as follows.

$$\begin{aligned}
\text{Odd sign pairing : } T_c &= \Lambda_{\text{ph}} \cdot \exp \left\{ -\frac{1 + \lambda_+}{\text{Max} \left[\lambda_- - V_-^* \left(1 + \lambda_- \frac{\langle \omega \rangle}{\Lambda_{\text{ph}}} \right), 0 \right]} \right\} \\
\text{Even sign pairing : } T_c &= \Lambda_{\text{ph}} \cdot \exp \left\{ -\frac{1 + \lambda_+}{\text{Max} \left[\lambda_+ - V_+^* \left(1 + \frac{\langle \omega \rangle}{\Lambda_{\text{ph}}} \right), 0 \right]} \right\}
\end{aligned} \tag{1}$$

where

$$\begin{aligned}
\lambda_{\pm} &= \lambda_{\text{intra}} \pm \lambda_{\text{inter}} \\
V_{\pm} &= V_{\text{intra}} \pm V_{\text{inter}} \\
V_{\pm}^* &= V_{\pm} / [1 + V_{\pm} \ln(\Lambda_e / \Lambda_{\text{ph}})].
\end{aligned} \tag{2}$$

Here ‘‘Odd’’/‘‘Even’’ sign pairing means the gap function has opposite/same sign on the two Fermi pockets. V_{intra} and V_{inter} are the average of the intra and inter-pocket Cooper scattering strength obtained from the first stage calculation. λ_{intra} and λ_{inter} are the strength of the phonon mediated Cooper scattering entering the second stage calculation. $\langle \omega \rangle$ is a weighted average[10] of the phonon frequency satisfying $0 < \langle \omega \rangle / \Lambda_{\text{ph}} < 1$. In obtaining the above result we have assumed that $1 + V_{\pm} \ln(\Lambda_e / \Lambda_{\text{ph}}) > 0$, i.e., the pure electronic driven T_c is lower than $\Lambda_{\text{ph}} / k_B$.

According to Eq.(1) increases $\lambda_{\text{intra}} - \lambda_{\text{inter}}$, and $V_{\text{inter}} - V_{\text{intra}}$ raises the T_c for the odd sign pairing. On the other hand, to raise the T_c of the even sign pairing we need to increase $\lambda_{\text{intra}} + \lambda_{\text{inter}}$ but decrease $V_{\text{intra}} + V_{\text{inter}}$, i.e.,

$$\begin{aligned}
(\lambda_{\text{intra}} - \lambda_{\text{inter}}) \nearrow \quad \text{and} \quad (V_{\text{inter}} - V_{\text{intra}}) \nearrow &\Rightarrow T_c^{\text{odd}} \nearrow \\
(\lambda_{\text{intra}} + \lambda_{\text{inter}}) \nearrow \quad \text{and} \quad (V_{\text{inter}} + V_{\text{intra}}) \searrow &\Rightarrow T_c^{\text{even}} \nearrow.
\end{aligned} \tag{3}$$

The physics behind Eq.(3) is rather simple. Odd/Even sign pairing *requires* the inter-pocket Cooper scattering to be repulsive/attractive. Since phonon mediated scattering is necessarily attractive, it follows that strong inter-pocket electron-phonon interaction enhances even sign pairing while suppress the odd sign pairing. Because attractive intra-pocket scattering strengthen both even and odd sign pairing, strong intra-pocket electron phonon interaction is beneficial to both.

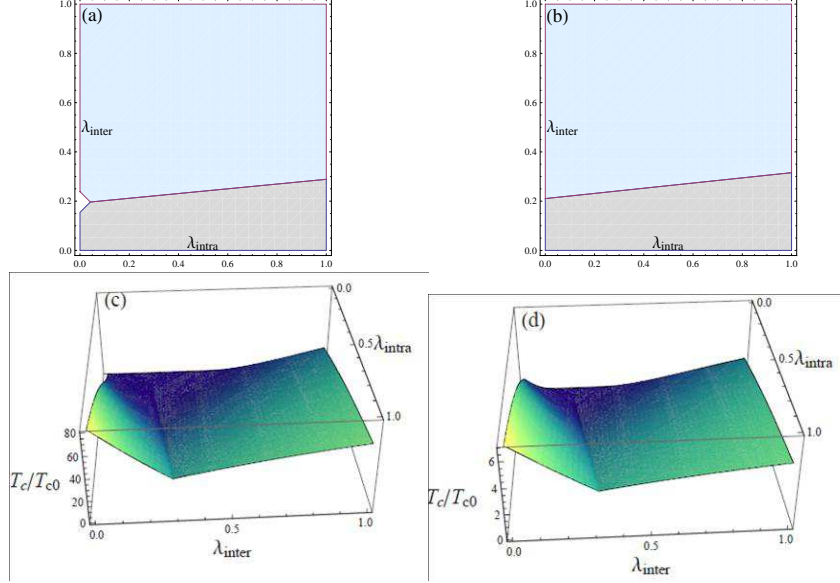


FIG. 2: (a,b) the phase diagram. Light blue/gray denote even/odd sign pairing, respectively. (c,d) the T_c enhancement factor T_c/T_{c0} where T_{c0} is the superconducting transition temperature in the absence of the electron-phonon interaction. The parameters we used to construct the figures are $\Lambda_e/\Lambda_{ph} = 2$, $\langle\omega\rangle/\Lambda_{ph} = 0.5$, and $V_{inter} = 0.2$, $V_{intra} = 0.05$ for (a) and (c), and $V_{inter} = 0.2$, $V_{intra} = -0.05$, for (b) and (d). The small triangular region near the lower left hand corner of panel (a) is non-superconducting.

A. The undoped FeSe/STO

For undoped FeSe/STO the first stage RG generates $V_{inter} > 0$ hence favoring odd sign (S_{+-}) pairing.[7, 8, 11] This is caused by the antiferromagnetic fluctuation. As discussed above, λ_{intra} enhances the S_{+-} pairing while λ_{inter} weakens it. Setting $V_{inter} = 0.2$ and $V_{intra} = \pm 0.05$, the “phase diagrams” as a function of λ_{intra} and λ_{inter} is shown in Fig. 2(a,b). The associated T_c enhancement factor is shown in Fig. 2(c,d). Note the magnitude of the T_c enhancement differs by approximately an order of magnitude in Fig. 2(c,d) by merely reversing the sign of V_{intra} . Clearly this quantity is not something we can confidently predict. What is robust is the fact that when $\lambda_{inter} \gg \lambda_{intra}$ electron-phonon interaction stabilizes even sign pairing. Conversely for $\lambda_{intra} \gg \lambda_{inter}$ odd sign pairing is favored. Since for undoped FeSe/STO the FE phonons mainly cause intra-pocket electron scattering ($\lambda_{intra} \gg \lambda_{inter}$), we expect the electron-phonon interaction to strengthen the odd sign, in this case S_{+-} , pairing.

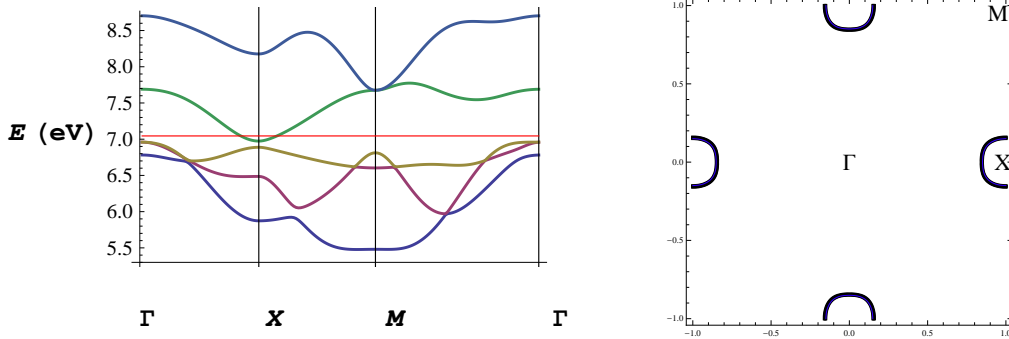


FIG. 3: Left: A tight-binding fit to the band dispersion observed in Ref.[2]. Right panel: the electron-like Fermi surfaces.

B. The electron doped FeSe/STO

Our tight-binding fit of the ARPES bandstructure and the associated Fermi surfaces are shown in Fig.3. Because the hole bands have completely sunk below the Fermi energy, the antiferromagnetic fluctuation only occurs at energies greater than the separation between the top of the hole bands and the Fermi energy. According Ref.[2] this separation is approximately 80 meV. If sufficiently strong this high energy magnetic fluctuation can trigger S_{++} pairing on the electron pockets. This pairing form factor can be thought of as S_{+-} restricted to the exposed Fermi surfaces. When this form factor is the leading pairing channel, we expect V_{intra} and V_{inter} to be both negative. Under this condition adding the electron-phonon interaction the phase diagram is shown in Fig. 4(a)- there is only S_{++} phase. The T_c enhancement is shown in Fig. 4(b).

For larger separation between the hole bands and E_F , the nodeless d-wave (where the gap function has opposite sign on the two electron pockets) is the leading pairing channel. As pointed out in Ref.[12] in the presence of hybridization between the electron pockets (due to the absence of the $z \leftrightarrow -z$ symmetry at the interface) the d-wave pairing can become nodal. For strong hybridization the reconstructed electron pockets could have opposite sign pairing due to the repulsive electron-electron interaction.[12, 13] We expect in both cases Fig. 2 should apply, i.e., strong enough inter-pocket scattering (the first main effect of the FE phonon in earlier discussions), can destabilize the odd sign pairing and turn it into even sign. In addition to the effect of phonon the inevitable disorder scattering also tends to destabilize the odd sign pairing in favor of even sign. Thus we strongly believe *the electron*

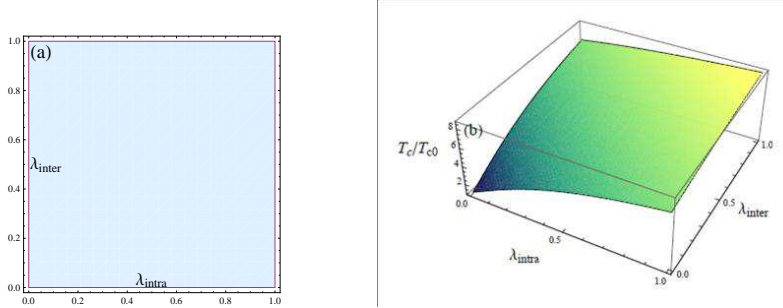


FIG. 4: (a) the phase diagram. Light blue denotes the even sign pairing. (b) the T_c enhancement factor T_c/T_{c0} where T_{c0} is the superconducting transition temperature in the absence of the electron-phonon interaction. The parameters we used to construct the figures are $\Lambda_e/\Lambda_{ph} = 2$, $\langle\omega\rangle/\Lambda_{ph} = 0.5$, and $V_{\text{intra}} = -0.2$, $V_{\text{inter}} = -0.05$.

doped FeSe/STO have even sign (or S_{++}) pairing.

Now we present the more technical part of the paper.

III. THE FIRST STAGE - FRG CALCULATION

The electronic Hamiltonian consists of the bandstructure part, H_{band} , and the Hubbard-Hundes interaction H_I . The details of H_I can be found in Appendix A. For the undoped FeSe/STO because of the well nested Fermi surfaces[3] particle-hole scattering is expected to grow continuously at low energies. As the result the assumption made earlier, that we only need to retain the Cooper channel electron-electron scattering for $E < \Lambda_{\text{ph}}$, is not a priori justified. Consequently in the next subsection we shall perform a full FRG treatment of both electrons and FE phonons to check the results obtained using the Eliashberg approach.

A. The undoped FeSe/STO

The Fermi surfaces (in the unfolded Brillouin zone) of the undoped system are shown in Fig. 5(a). The phonon Hamiltonian is given by $H_{\text{ph}} = \sum_{\mathbf{p}} \omega(\mathbf{p}) a_{\mathbf{p}}^\dagger a_{\mathbf{p}}$. Here \mathbf{p} is the three-dimensional momentum. We assume the following dispersion for the FE phonon $\omega(\mathbf{p}) = \sqrt{\omega_0^2 + c^2 p^2}$ where $\omega_0 \approx 2\text{meV}$ and $c \sim 70\text{meV} \cdot \text{\AA}$ are estimated from an early neutron

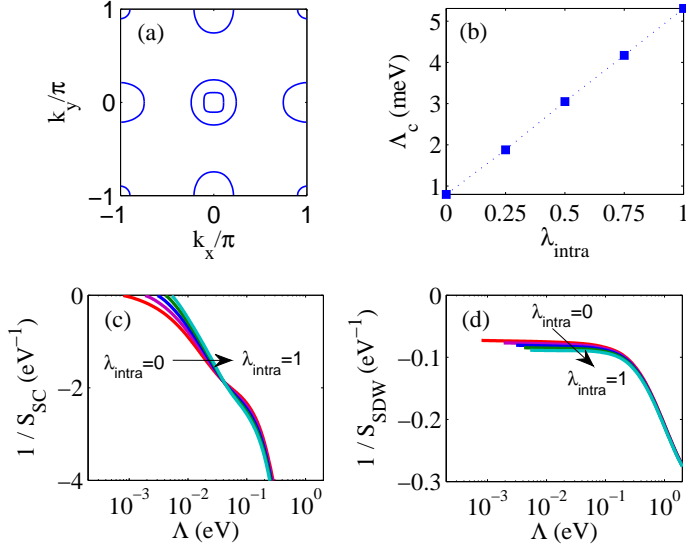


FIG. 5: (a) FeSe Fermi surface(s). (b) The superconducting critical scale Λ_c versus λ_{intra} . (c) and (d) presents the flow of S_{SC} and S_{SDW} , respectively. (Higher scales are not shown). The value of λ_{intra} increases by equal intervals along the arrows.

measurement.[14] The electron-phonon Hamiltonian is given by

$$H_{e\text{-ph}} = A \sum_{i,\alpha} u_i n_{i\alpha} \rightarrow \sum_{p_z} \sum_{\mathbf{k}a,\mathbf{k}'b} g_{\mathbf{k}a,\mathbf{k}'b;p_z} (a_{\mathbf{k}-\mathbf{k}'+\mathbf{p}_z}^\dagger + a_{\mathbf{k}'-\mathbf{k}-\mathbf{p}_z}) \Psi_{\mathbf{k}'b}^\dagger \tau_3 \Psi_{\mathbf{k}a}. \quad (4)$$

$H_{e\text{-ph}}$ describes the coupling between electrons in the FeSe layer and the nearest ion displacement u_i in the TiO_2 layer of STO. In the above $\mathbf{p}_z = p_z \hat{z}$ is the out-of-plane momentum of the phonon and τ_3 is the third Pauli matrix in the Nambu space. The summation over p_z follows from the fact that the electron-phonon coupling occurs at the interface. Here a and b label the electron bands, and $g_{\mathbf{k}a,\mathbf{k}'b;p_z} \propto A \langle \mathbf{k}a | \mathbf{k}'b \rangle / \sqrt{\omega(\mathbf{k}-\mathbf{k}'+\mathbf{p}_z)}$ where $\langle \mathbf{k}a | \mathbf{k}'b \rangle$ is the overlap between band Bloch states. The phonon mediated intra and inter-pocket Cooper scattering strength are given by $\lambda_{\text{intra}} = \sum_{a=1}^5 \lambda_{aa}/5$ and $\lambda_{\text{inter}} = \sum_{a \neq b} \lambda_{ab}/20$, where

$$\lambda_{ab} = \sqrt{N_a N_b} \sum_{p_z} \langle \langle \frac{2|g_{\mathbf{k}a,\mathbf{k}'b;p_z}|^2}{\omega(\mathbf{k}-\mathbf{k}'+\mathbf{p}_z)} \rangle \rangle_{a,b}, \quad (5)$$

where $\langle \langle \cdot \rangle \rangle$ denotes the joint average over \mathbf{k} and \mathbf{k}' which lie on Fermi pockets a and b respectively. Using ω_0 and c above and the Fermi pockets in Fig. 5(a) we estimate $\lambda_{\text{inter}}/\lambda_{\text{intra}} \sim 1/12$.

We generalize the SM-FRG method[15, 16] to treat the effects of both electron-electron and electron phonon interactions. In principle, we envision a boson-fermion FRG calculation

that involves the flow of electron self energy, the phonon self energy, the electron-phonon coupling vertex, the 4-point phonon vertex, as well as the electron-electron interaction vertex. However in the following shall view the electron dispersion, the phonon dispersion, and the electron-phonon coupling as fully renormalized quantities. The first two can be determined from experiments and the last quantity is viewed as an adjustable parameter in our theory. What's left is the RG flow of the electron-electron interaction including contributions from the pure electron-electron interaction and the phonon mediated interaction. In the following the renormalized interactions in the superconducting (SC) and spin density wave (SDW) channels are denoted as $S_{SC,SDW}$. (The charge density wave channel turns out to be unimportant and will not be discussed.) The definitions as well as technical details of the SM-FRG method can be found in Appendix A.

Fig. 5(b) summarizes the superconducting critical scale Λ_c (filled squares) versus the electron-phonon interaction parameter λ_{intra} ($\lambda_{\text{inter}} \sim \lambda_{\text{intra}}/12$). This is extracted from Fig. 5(c) which shows the flow of S_{SC} . Fig. 5(b) shows a linearly rising Λ_c as a function of λ_{intra} . When we compare the maximum Λ_c with that in the absence of electron-phonon interaction a maximum T_c enhancement ~ 6.5 is obtained. Given the fact that $\lambda_{\text{intra}} \sim 12\lambda_{\text{inter}}$ this result is consistent with Fig. 2. We have checked that for all values of λ_{intra} in Fig. 5(c) the pairing symmetry remains to be S_{+-} . Fig. 5(d) shows that the S_{SDW} almost saturates at low energy scales, and the electron-phonon coupling reduces $1/S_{SDW}$ only slightly. Since this type of SDW is related to the pairing interaction, the above observation justifies our previous assumptions for the input to the Eliashberg calculation.

B. The electron doped FeSe/STO

In this case the assumption of only retaining the Cooper channel electron-electron scattering is a good approximation. Hence we shall focus on the pure electronic calculation to find out the leading pairing channels and use it as input for the second stage Eliashberg calculation. The electronic structure we use to describe the electron doped FeSe is shown in Fig. 3. It is worthy to note that this bandstructure differs substantially from those for other pnictides in that the hole band top near Γ and the electron band bottom near X and Y are separated by a small gap. Interesting in a recent ARPES work on $A_xFe_ySe_2$ [17] this feature is noted and emphasized.

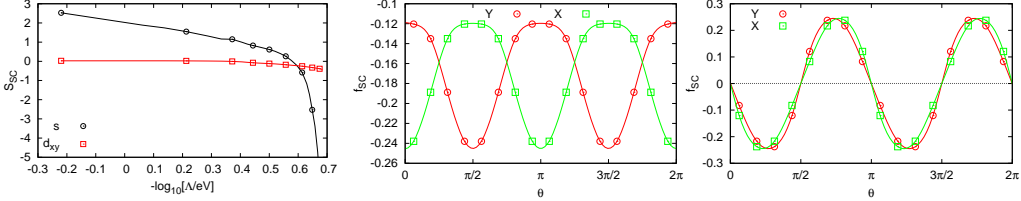


FIG. 6: Left panel: the RG flow of the Cooper scattering strength S_{SC} associated with the two leading pairing channels. Black circles: s-wave pairing. Red squares: d_{xy} pairing. Mid panel: the s-wave form factor. The polar angle θ is defined with respect to the $+x$ direction for both $X(\pi, 0)$ and $Y(0, \pi)$ electron pockets. Right panel: the d_{xy} form factor.

For $(U, U', J_H) = (2, 1.7, 0.15)$ eV, the FRG results for the Cooper pairing is shown in Fig. 6. The left panel shows the leading pairing instability being in the s-wave channel (black), while the subleading pairing channel has d_{xy} symmetry (red). The form factors for the s and d_{xy} pairing are shown in mid and right panels respectively. For the s-wave pairing, the form factor has the same sign on the two electron pockets X and Y. However the amplitude of the form factor is quite anisotropic. In contrast the d_{xy} form factor has nodes on the two electron pockets. We have also checked for considerably weaker interaction parameters, the leading pairing channel is $d_{x^2-y^2}$ where the gap function has opposite sign on the X and Y electron pockets. As discussed earlier, the interaction with FE phonon tends to stabilize the s wave pairing and suppress the d-wave pairing. For intermediate electron-electron interaction parameters we obtain s-wave pairing. The addition of FE phonons will further enhance the pairing energy scale.

IV. THE SECOND STAGE - THE ELIAHBERG EQUATIONS

The formalism and notations in this section closely follow those in Scalapino *et al.*[18] and McMillan [10]. The details can be found in Appendix B. In order to make analytic calculation feasible, we model the low energy electronic degrees of freedom by two Fermi surfaces. In the case of undoped FeSe these correspond to hole and electron pockets and for the electron doped case both Fermi surfaces correspond to electron pockets. These two Fermi surfaces are labeled by $a = 1, 2$ in (B1) respectively. Moreover we shall assume these Fermi surfaces have constant density of states(DOS) $N_{1,2}$. In addition, in the rest of this section the interaction $V_{abcd}(\mathbf{p}_1, \mathbf{p}_2, \mathbf{p}_3, \mathbf{p}_4)$ will be assumed to depend on the Fermi surface

index only, *i.e.*, V_{abcd} . These simplifications are made in view of the presumably strong disorder-induced quasiparticle scattering at the FeSe/STO interface which will average out the fine structures in $V_{abcd}(\mathbf{p}_1, \mathbf{p}_2, \mathbf{p}_3, \mathbf{p}_4)$ and the DOS.

Assume the following form for the self energy of the Nambu spinor Ψ ,

$$\Sigma_a(\omega) = [1 - Z_a(\omega)]\omega\tau_0 + Z_a(\omega)\Delta_a(\omega)\tau_1, \quad (6)$$

we derive the self-consistent equations for Z and Δ following standard procedures.[18] The results are given by Eqs. (B7) and (B8) in Appendix B. Assuming the McMillan ansatz (Eqs (B9)) these equation can be solved to yield $Z_a(0) = 1 + \sum_b \sqrt{N_b/N_a}\lambda_{ab}$ for the normal state $Z_a(0)$, and the following eigenvalue problem for T_c (B8)

$$\begin{aligned} \sum_{b=1}^2 \lambda_{ab} \left[\ln \frac{\Lambda_{\text{ph}}}{T_c} \cdot \sqrt{N_b}\Delta_b(0) + \frac{\langle\omega\rangle_{ab}}{\Lambda_{\text{ph}}} \cdot \sqrt{N_b}\Delta_b(\infty) \right] + \sqrt{N_a}\Delta_a(\infty) &= \sqrt{N_a}Z_a(0)\Delta_a(0), \\ - \sum_{b=1}^2 v_{ab} \left[\ln \frac{\Lambda_{\text{ph}}}{T_c} \cdot \sqrt{N_b}\Delta_b(0) + \ln \frac{\Lambda_e}{\Lambda_{\text{ph}}} \cdot \sqrt{N_b}\Delta_b(\infty) \right] &= \sqrt{N_a}\Delta_a(\infty). \end{aligned} \quad (7)$$

In the above equations $\lambda_{ab} = 2 \int_0^\infty \frac{d\nu}{\nu}$ and $\alpha_{ab}^2(\nu)F(\nu)$, where $F(\nu)$ is the density of states associated with the phonon mode and $\alpha_{ab}^2(\nu)$ is the effective electron-phonon coupling constants. In addition $v_{ab} = \sqrt{N_a N_b} V_{abba}$, and $\langle\omega\rangle_{ab}$ is a weighted average [weighted by $\alpha_{ab}^2(\nu)F(\nu)/\nu$] of the phonon frequency. See Appendix B for details.

For the sake of simplicity we shall set $N_1 = N_2$, $\lambda_{aa} \rightarrow \lambda_{\text{intra}} = (\lambda_{11} + \lambda_{22})/2$, $\lambda_{ab} \rightarrow \lambda_{\text{inter}} = (\lambda_{12} + \lambda_{21})/2$, $v_{aa} \rightarrow v_{\text{intra}} = (v_{11} + v_{22})/2$, $v_{ab} \rightarrow v_{\text{inter}} = (v_{12} + v_{21})/2$, and $\langle\omega\rangle_{ab} = \langle\omega\rangle$ in the following. With the above simplifications we can determine the T_c for S_{+-} ($\Delta_1 = -\Delta_2$) and S_{++} ($\Delta_1 = \Delta_2$) pairing as given by Eq. (1). We have checked changing N_1/N_2 has little effect on T_c while have a strong effect on Δ_1/Δ_2 .

If phonons are indeed responsible for the observed T_c enhancement, there should be other signatures of the electron-phonon coupling. For example due to the large anharmonicity of the FE phonons we expect using a pump laser to excite them will have a clear effect on T_c . The more traditional phonon signatures such as kink in the quasiparticle dispersion and shoulder in the tunneling experiment are discussed in Appendix C.

V. DISCUSSION

We have studied the screening effects the ferroelectric phonons of SrTiO₃ on the interaction between the electrons in FeSe. We conclude such coupling can enhance the pairing

strength of FeSe. Moreover we find when the inter-pocket electron-phonon scattering is strong, the opposite sign pairing will give way to the equal sign pairing.

An immediate question one might ask is why don't the FE phonons have similar effect on the T_c of doped STO. We believe the answer is polaron formation - for a range of strong electron-phonon coupling, the formation of polarons instead of Cooper pairs are favored. In a recent optical experiment on n-type doped STO,[19] a very sharp Drude peak with a substantial mass enhancement (consistent with that of "large polarons") was observed.

The current study raises the concern about whether the role of phonon can be completely ignored in bulk iron-based superconductors.[20] With appropriate interpretation of λ_{intra} and λ_{inter} , our results can be used to address the phonon effects in bulk iron-based superconductors as well.

Material wise there are other nearly ferroelectric perovskite materials, for example KTaO_3 . [21] If FeSe films can be epitaxially grown on these materials similar T_c enhancement should occur. Finally the results of Ref.[1] and the present paper suggest the ... $\text{FeSe}/(\text{STO})_n/\text{FeSe}/(\text{STO})_n\dots$ superlattice is a promising artificial material with high T_c .

Acknowledgments

We are in debt to Yuan-Ming Lu who helped us understand the phonons in SrTiO_3 , and Fan Yang for informing us of the experimental result of Ref.[1]. We thank Qi-Kun Xue and Xingjiang Zhou for sharing their unpublished results with us, and R. Ramesh for telling us many important properties of SrTiO_3 . We also thank Todadri Senthil, Tao Xiang, Jun Zhao and Yuan Wan for helpful discussions. QHW acknowledges the support by the Ministry of Science and Technology of China (under grant No.2011CBA00108 and 2011CB922101) and NSFC (under grant No.10974086, No.10734120 and No.11023002). DHL acknowledges the support by the DOE grant number DE-AC02-05CH11231.

Appendix A: The SM-FRG method

In this section we describe the SM-FRG method we used. The microscopic hamiltonian, which is valid for all cutoff $<$ bandwidth, we use is $H = H_{\text{band}} + H_I + H_{\text{ph}} + H_{\text{e-ph}}$. Here H_{band} is the two dimensional bandstructure. For the undoped case H_{band} is a courtesy of

Z-Y Lu.[22] For the electron doped case it obtained by a fit to the ARPES result[2]. H_I describes the local electron-electron interaction given by

$$\begin{aligned}
H_I = & U \sum_{i,\alpha} n_{i,\alpha,\uparrow} n_{i,\alpha,\downarrow} + U' \sum_{i,\alpha>\beta} n_{i,\alpha} n_{i,\beta} + J_H \sum_{i,\alpha>\beta,\sigma,\sigma'} \psi_{i,\alpha,\sigma}^\dagger \psi_{i,\beta,\sigma} \psi_{i,\beta,\sigma'}^\dagger \psi_{i,\alpha,\sigma'} \\
& + J_H \sum_{i,\alpha>\beta} (\psi_{i,\alpha,\uparrow}^\dagger \psi_{i,\alpha,\downarrow}^\dagger \psi_{i,\beta,\downarrow} \psi_{i,\beta,\uparrow} + \text{h.c.}), \tag{A1}
\end{aligned}$$

where $\psi_{i,\alpha,\sigma}$ annihilates a spin σ electron at site i in orbital α ($\alpha = 3z^2 - r^2, xz, yz, x^2 - y^2, xy$), $n_{i,\alpha,\sigma} = \psi_{i,\alpha,\sigma}^\dagger \psi_{i,\alpha,\sigma}$ and $n_{i,\alpha} = \sum_{\sigma} n_{i,\alpha,\sigma}$. In the calculation of the main text we used intra-orbital repulsion $U = 2eV$, Hund's rule coupling $J_H = 0.31eV$, and inter-orbit repulsion $U' = U - 2J_H$.

Fig. 7 (a) shows a generic 4-point vertex function Γ_{1234} which appears in the interaction $\psi_1^\dagger \psi_2^\dagger (-\Gamma_{1234}) \psi_3 \psi_4$. Here 1, 2, 3, 4 represent momentum (or real space position) and orbital label. The spin σ and τ are conserved along fermion propagators and will be suppressed henceforth. Figs.7(b)-(d) are rearrangements of (a) into the pairing (P), the crossing (C) and the direct (D) channels in such a way that a collective momentum \mathbf{q} can be identified. The dependence on all other momenta and orbital labels is written as

$$\begin{aligned}
\Gamma_{\mathbf{k}+\mathbf{q},-\mathbf{k},-\mathbf{p},\mathbf{p}+\mathbf{q}}^{\alpha\beta\gamma\delta} & \rightarrow \sum_{mn} f_m^*(\mathbf{k}, \alpha, \beta) P_{mn}(\mathbf{q}) f_n(\mathbf{p}, \delta, \gamma), \\
\Gamma_{\mathbf{k}+\mathbf{q},\mathbf{p},\mathbf{k},\mathbf{p}+\mathbf{q}}^{\alpha\beta\gamma\delta} & \rightarrow \sum_{mn} f_m^*(\mathbf{k}, \alpha, \gamma) C_{mn}(\mathbf{q}) f_n(\mathbf{p}, \delta, \beta), \\
\Gamma_{\mathbf{k}+\mathbf{q},\mathbf{p},\mathbf{p}+\mathbf{q},\mathbf{k}}^{\alpha\beta\gamma\delta} & \rightarrow \sum_{mn} f_m^*(\mathbf{k}, \alpha, \delta) D_{mn}(\mathbf{q}) f_n(\mathbf{p}, \gamma, \beta). \tag{A2}
\end{aligned}$$

Here $f_{m=(l,o)}(\mathbf{k}, \alpha, \beta) = h_l(\mathbf{k}) \mathcal{M}_o(\alpha, \beta)$ is a composite form factor, where $h_l(\mathbf{k})$ is chosen from a set of orthonormal lattice harmonics, \mathcal{M}_o is a matrix in the orbital basis.

The decomposition Eq. (A2) for each channel would be exact if the form factor set is complete. In practice, however, a set of a few form factors is often sufficient to capture the symmetry of the order parameters associated with leading instabilities.[15, 16] In our case, the lattice harmonics are chosen as $h(\mathbf{k}) = 1, \cos k_x \pm \cos k_y, 2 \cos k_x \cos k_y$ and $2 \sin k_x \sin k_y$. They are all even since only singlet pairing is relevant in our case. The \mathcal{M} -matrices are chosen so that the combination $\sum_{\alpha\beta} \phi_\alpha \mathcal{M}(\alpha, \beta) \phi_\beta$ (ϕ_α is the real atomic orbital function) is irreducible and transforms according to A_{1g}, B_{1g} or B_{2g} under the point group.[23] (One may also use any bilinear $\phi_\alpha \phi_\beta$ to determine a matrix \mathcal{M} , but it is less transparent symmetry wise.) Moreover, the \mathcal{M} -matrix is normalized as $\text{Tr} \mathcal{M}^\dagger \mathcal{M} = 1$. If the total number of

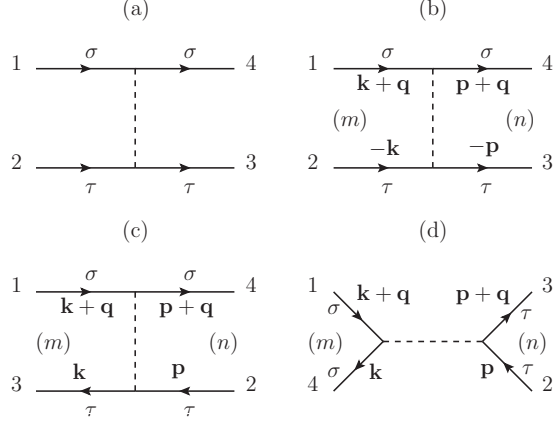


FIG. 7: A generic 4-point vertex (a) is rearranged into the pairing (b), crossing (c) and direct (d) channels. Here $\mathbf{k}, \mathbf{q}, \mathbf{p}$ are momenta, σ and τ denote spins which are conserved during fermion propagation, and m, n denote the form factor (see the text for details).

composite form factors is N , then P , C and D are all $N \times N$ matrix functions of \mathbf{q} . Note that the P, C and D channels are not orthogonal. The overlap between different channels are important for the growth of pairing interaction out of, e.g., the magnetic interaction.[7, 9, 16] In the following we denote $X_K = \hat{K}X$ as the projection of X into the K-channel via Eq. (A2).

In the case with electron-phonon interaction we need the phonon-mediated electron-electron scattering. According to the H_{e-ph} defined in the text, this vertex is given by,

$$V(\mathbf{q}, \nu_n) \propto \sum_{p_z} \frac{A^2}{\nu_n^2 + \omega^2(\mathbf{q} + p_z \hat{z})} \propto \frac{A^2}{\sqrt{\nu_n^2 + \omega^2(\mathbf{q})}}, \quad (\text{A3})$$

where $\mathbf{q} = (q_x, q_y)$ and ν_n are the momentum and (Matsubara) frequency transfer in the electron-electron scattering, and the last proportionality holds to leading order in ω_0/c . The $\lambda_{\text{intra,inter}}$ discussed in the main text are both proportional to A^2 . Notice that this vertex is naturally in the D -channel and bears trivial form factors with $h = 1$ and $\mathcal{M} = \delta_{\alpha\beta}$ since according to Eq. (4) the electron-phonon interaction is local in real space and diagonal in orbital basis.

The partial flows of P , C and D are given by the one-particle-irreducible diagrams shown in Fig. 8. Here the dashed line denotes 4-point fermion vertex, wavy line the (surface) phonon-mediated vertex, and the dash-wavy line means that both types of vertices can enter. We write the partial flow equations as, in matrix form and for a collective momentum

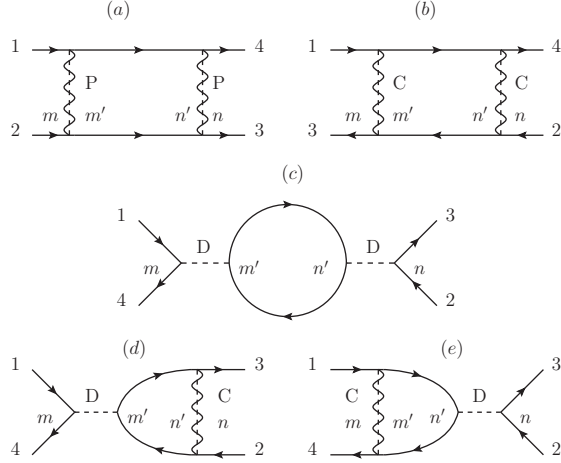


FIG. 8: One-loop diagrams contributing to the flow of the the 4-point vertex function in the pairing channel (a), crossing channel (b), and direct channel (c)-(e). Here m, m', n, n' denote form factors, while the momentum, orbital and spin indices are left implicit. The dashed line represent 4-point fermion vertex, dash-wavy line means that both fermion vertex and phonon propagator can be inserted but separately. The diagrams are one-particle-irreducible with respect to both fermions and phonons, and the phonon line shares the loop frequency since external fermion fields are set at zero frequency as usual. The Matsubara frequency is continuous but subject to hard infrared cutoff at running scale Λ .

\mathbf{q} ,

$$\begin{aligned}
\frac{\partial P}{\partial \Lambda} &= (P + V_P) \chi'_{pp} (P + V_P), \\
\frac{\partial C}{\partial \Lambda} &= (C + V_C) \chi'_{ph} (C + V_C), \\
\frac{\partial D}{\partial \Lambda} &= (C + V_C - D) \chi'_{ph} D + D \chi'_{ph} (C + V_C - D).
\end{aligned} \tag{A4}$$

Here Λ is the running Matsubara frequency cutoff, V_K is the phonon mediated interaction projected into the K channel at cutoff Λ , and $\chi'_{pp/ph}$ are matrix-kernels with elements

$$\begin{aligned}
(\chi'_{pp})_{mn} &= -\frac{1}{2\pi} \int \frac{d^2 \mathbf{p}}{(2\pi)^2} f_m(\mathbf{p}, \alpha, \beta) G_{\alpha\gamma}(\mathbf{p} + \mathbf{q}, i\Lambda) G_{\beta\delta}(-\mathbf{p}, -i\Lambda) f_n^*(\mathbf{p}, \gamma, \delta) + (\Lambda \rightarrow -\Lambda), \\
(\chi'_{ph})_{mn} &= -\frac{1}{2\pi} \int \frac{d^2 \mathbf{p}}{(2\pi)^2} f_m(\mathbf{p}, \alpha, \beta) G_{\alpha\gamma}(\mathbf{p} + \mathbf{q}, i\Lambda) G_{\delta\beta}(\mathbf{p}, i\Lambda) f_n^*(\mathbf{p}, \gamma, \delta) + (\Lambda \rightarrow -\Lambda)
\end{aligned} \tag{A5}$$

where G is the bare fermion propagator in the orbital basis, and the summation over orbitals is left implicit.

Clearly, because of the Λ dependence, the effect of phonon mediated interaction, V , is important only if Λ reaches the phonon band, above which the main contribution to the flow of the fermion interaction vertex is from pure electron-electron interaction. However the electronic excitations do modify phonon self energy and electron-phonon vertex even when the cutoff scale is above the phonon bandwidth. In the present work such effects are accounted for by using the experimentally measured phonon dispersion and the electron-phonon coupling constant. The flows in Eq. (A4) collect contributions from independent one-particle-irreducible diagrams for the total change $d\Gamma$, which need to be subsequently projected to the three channels. Therefore the full flow equations can be formally written as,

$$\frac{dK}{d\Lambda} = \frac{\partial K}{\partial \Lambda} + \hat{K} \sum_{K' \neq K} \frac{\partial K'}{\partial \Lambda}, \quad (\text{A6})$$

for $K = P, C$ and D . We used the fact that $\hat{K} \partial K = \partial K$ by definition.

The functions P , C and D are related to the effective interactions as, $V_{sc} = -P - V_P$ in SC-, $V_{sdw} = C + V_C$ in SDW-, and $V_{cdw} = C + V_C - 2D$ in CDW-channels. We monitor the most negative singular values $S_{SC,SDW,CDW}$ of such interactions (for all \mathbf{q}) versus the running cutoff Λ . The most negative one among $S_{SC,SDW,CDW}$ tells us which channel is becoming unstable. The associated eigen function dictates the symmetry and wave vector of the order parameter.

Appendix B: Multiple band Eliashberg equation

In this Appendix we briefly outline the derivation of multiple band Eliashberg equations for the electron-phonon Hamiltonian (B1), following the single band case of Scalapino *et al.* [18]

The effective electron-phonon Hamiltonian we consider, at the energy cutoff Λ_e , is given by

$$\begin{aligned} H = & \sum_{a=1}^2 \sum_{\mathbf{p}} \epsilon_{\mathbf{p}a} \Psi_{\mathbf{p}a}^\dagger \tau_3 \Psi_{\mathbf{p}a} + \sum_{\mathbf{q}} \omega(\mathbf{q}) a_{\mathbf{q}}^\dagger a_{\mathbf{q}} \\ & + \sum_{a,b} \sum_{\mathbf{p},\mathbf{p}'} g_{\mathbf{p}\mathbf{p}',ab} \varphi_{\mathbf{p}-\mathbf{p}'} \Psi_{\mathbf{p}'b}^\dagger \tau_3 \Psi_{\mathbf{p}a} \\ & + \frac{1}{2} \sum_{a,b,c,d} \sum_{\mathbf{p}_1, \mathbf{p}_2, \mathbf{p}_3} V_{abcd}(\mathbf{p}_1, \mathbf{p}_2, \mathbf{p}_3, \mathbf{p}_4) (\Psi_{\mathbf{p}_3c}^\dagger \tau_3 \Psi_{\mathbf{p}_1a}) (\Psi_{\mathbf{p}_4d}^\dagger \tau_3 \Psi_{\mathbf{p}_2b}). \end{aligned} \quad (\text{B1})$$

Here Λ_e is much smaller than the bandwidth but larger than maximal phonon frequency Λ_{ph} , $\Psi_{\mathbf{p}a}$ is the Nambu spinor for electron band a with dispersion $\epsilon_{\mathbf{p}a}$, $a_{\mathbf{q}}$ is the destruction operator for phonon with dispersion $\omega(\mathbf{q})$, $\varphi_{\mathbf{q}} = a_{\mathbf{q}}^\dagger + a_{-\mathbf{q}}$, $\mathbf{p}_4 = \mathbf{p}_1 + \mathbf{p}_2 - \mathbf{p}_3$, τ_3 is the Pauli matrix, and $V_{abcd}(\mathbf{p}_1, \mathbf{p}_2, \mathbf{p}_3, \mathbf{p}_4)$ is the (effective) electron-electron interaction. Different levels of simplification will be applied to Eq. (B1), which will be discussed in more details in the following.

Assume the Green's function of Nambu spinor Ψ to be given by

$$[G_a(\mathbf{p}, \omega)]^{-1} = \omega - \epsilon_{\mathbf{p}a}\tau_3 - \Sigma_a(\mathbf{p}, \omega). \quad (\text{B2})$$

The self-consistent equation of the self-energy $\Sigma_a(\mathbf{p}, \omega)$ is

$$\begin{aligned} \Sigma_a(\mathbf{p}, i\omega) = -T \sum_{\omega', \mathbf{p}'} \sum_b \tau_3 G_b(\mathbf{p}', i\omega') \tau_3 \cdot \left[|g_{\mathbf{p}\mathbf{p}', ab}|^2 D(\mathbf{p} - \mathbf{p}', i\omega - i\omega') \right. \\ \left. + V_{abba}(\mathbf{p}, \mathbf{p}', \mathbf{p}', \mathbf{p}) \right] \end{aligned} \quad (\text{B3})$$

where ω' is fermion Matsubara frequency. $D(\mathbf{q}, \nu)$ is the Green's function of the phonon.

Use the spectral representation

$$D(\mathbf{q}, i\nu') = \int_0^\infty d\nu B(\mathbf{q}, \nu) \left[\frac{1}{i\nu' - \nu} - \frac{1}{i\nu' + \nu} \right], \quad (\text{B4})$$

and sum over ω' by the procedure of Ref. [18], the self-consistent equation becomes

$$\begin{aligned} \Sigma_a(\mathbf{p}, \omega) = - \sum_b \frac{1}{\pi} \sum_{\mathbf{p}'} \int_{-\infty}^\infty d\omega'' \text{Im}[\tau_3 G_b(\mathbf{p}', \omega'') \tau_3] \\ \times |g_{\mathbf{p}\mathbf{p}', ab}|^2 \int_0^\infty d\nu B(\mathbf{p} - \mathbf{p}', \nu) \left[\frac{N(\nu) + f(-\omega'')}{\omega - \omega'' - \nu} + \frac{N(\nu) + f(\omega'')}{\omega - \omega'' + \nu} \right] \\ - \sum_b \frac{1}{\pi} \sum_{\mathbf{p}'} \int_{-\infty}^{+\infty} d\omega'' \text{Im}[\tau_3 G_b(\mathbf{p}', \omega'') \tau_3] \frac{1}{2} V_{abba}(\mathbf{p} - \mathbf{p}') \tanh(\beta\omega''/2) \end{aligned} \quad (\text{B5})$$

Assume each electron band a has a circular Fermi surface with constant DOS N_a , define $\alpha_{ab}^2(\nu)F(\nu)$ as the average of $\sqrt{N_a N_b} |g_{\mathbf{p}\mathbf{p}', ab}|^2 B(\mathbf{p} - \mathbf{p}', \nu)$ over \mathbf{p} on Fermi surface a and \mathbf{p}' on Fermi surface b , and ignore the momentum dependence of Σ close to Fermi surface, this

equation further simplifies to

$$\begin{aligned}
\sqrt{N_a}\Sigma_a(\omega) = & \sum_b \sqrt{N_b} \int_{-\Lambda_e}^{\Lambda_e} d\epsilon_{p',b} \left\{ \right. \\
& - \frac{1}{\pi} \int_{-\infty}^{\infty} d\omega'' \int_0^{\infty} d\nu \alpha_{ab}^2(\nu) F(\nu) \text{Im}[\tau_3 G_b(p', \omega'') \tau_3] \\
& \times \left[\frac{N(\nu) + f(-\omega'')}{\omega - \omega'' - \nu} + \frac{N(\nu) + f(\omega'')}{\omega - \omega'' + \nu} \right] \\
& \left. - \frac{1}{\pi} \int_{-\infty}^{+\infty} d\omega'' \text{Im}[\tau_3 G_b(p', \omega'') \tau_3] \frac{1}{2} v_{ab} \tanh(\beta\omega''/2) \right\}.
\end{aligned} \tag{B6}$$

Here $N(\nu) = 1/(e^{\beta\nu} - 1)$ and $f(\omega) = 1/(e^{\beta\omega} + 1)$ are the Bose and Fermi distribution functions, $v_{ab} = \sqrt{N_a N_b} V_{abba}$. Assume that Σ_a takes the form of (6), the above equation reduces to

$$\begin{aligned}
\sqrt{N_a}[1 - Z_a(\omega)] = & \sum_b \sqrt{N_b} \int_0^{\infty} d\nu \alpha_{ab}^2(\nu) F(\nu) \int_0^{\Lambda_e} d\omega' \text{Re} \left[\frac{\omega'}{\sqrt{\omega'^2 - \Delta_b^2(\omega')}} \right] \\
& \times 2 \left[\frac{N(\nu) + f(-\omega')}{\omega^2 - (\omega' + \nu)^2} + \frac{N(\nu) + f(\omega')}{\omega^2 - (\omega' - \nu)^2} \right],
\end{aligned} \tag{B7}$$

and

$$\begin{aligned}
\sqrt{N_a}Z_a(\omega)\Delta_a(\omega) = & - \sum_b \sqrt{N_b} \int_0^{\infty} d\nu \alpha_{ab}^2(\nu) F(\nu) \int_0^{\Lambda_e} d\omega' \text{Re} \left[\frac{\Delta_b(\omega')}{\sqrt{\omega'^2 - \Delta_b^2(\omega')}} \right] \\
& \times 2 \left[\frac{(\omega' + \nu)[N(\nu) + f(-\omega')]}{\omega^2 - (\omega' + \nu)^2} + \frac{(\omega' - \nu)[N(\nu) + f(\omega')]}{\omega^2 - (\omega' - \nu)^2} \right] \\
& - \sum_b \sqrt{N_b} \int_0^{\Lambda_e} d\omega' \text{Re} \left[\frac{\Delta_b(\omega')}{\sqrt{\omega'^2 - \Delta_b^2(\omega')}} \right] v_{ab} \tanh(\beta\omega'/2).
\end{aligned} \tag{B8}$$

These equations can be solved numerically for the frequency dependence of Z and Δ . For a more transparent demonstration of the physics, we adopt the McMillan approximation [10] and look for solutions of the form

$$\begin{aligned}
Z_a(\omega < \Lambda_{\text{ph}}) &= Z_a(0), & Z_a(\omega > \Lambda_{\text{ph}}) &= 1, \\
\Delta_a(\omega < \Lambda_{\text{ph}}) &= \Delta_a(0), & \Delta_a(\omega > \Lambda_{\text{ph}}) &= \Delta_a(\infty).
\end{aligned} \tag{B9}$$

This leads to the generalized McMillan formula (7) in main text.

Appendix C: The phonon signatures

Conventional signatures of the electron-phonon interaction include the phonon induced kink in the normal state dispersion and the phonon shoulder in the tunneling spectra. How-

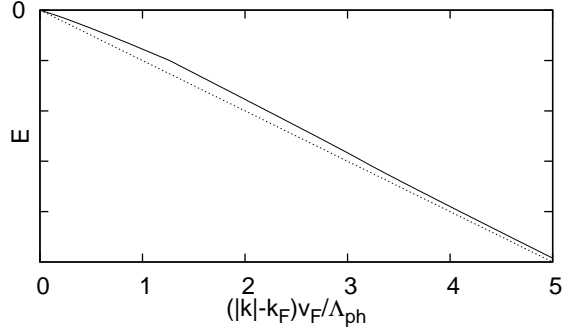


FIG. 9: Solid(dash) line is the renormalized(un-renormalized) electron dispersion, obtained by numerical solution of (B7) with parameters $\lambda_{\text{intra}} = 0.5$ and $\lambda_{\text{inter}} = 0$, and the model of FE phonon described in Section III. No prominent kink is visible despite significant (factor 1.5) mass enhancement at Fermi level.

ever these features are most pronounced when $\alpha^2(\nu)F(\nu)$ have a sharp peak at a characteristic phonon frequency. While this is indeed the case for Einstein phonons it is not true for the soft phonons under discussion. Here we expect $\alpha^2(\nu)F(\nu)$ to have a wide distribution. Therefore the above phonon features may not be very obvious. For example using the parameters described in the main text a typical renormalized quasiparticle dispersion in the normal state near the Fermi surface is shown in Fig. 9.

-
- [1] Q.-Y. Wang *et al.*, Chin. Phys. Lett. **29**, 037402 (2012).
 - [2] Defa Liu *et al.*, arXiv:1202.5849.
 - [3] Kai Liu, Zhong-Yi Lu, and Tao Xiang, arXiv:1202.0538.
 - [4] G. T. Zimanyi, S. A. Kivelson, and A. Luther, Phys. Rev. Lett. **60**, 2089 (1988).
 - [5] H. Fu, C. Honerkamp and D.-H. Lee, , Europhys. Lett. **76** 146 (2006).
 - [6] C. Honerkamp, M. Salmhofer, N. Furukawa, T. M. Rice, Phys. Rev. B 63, 035109 (2001).
 - [7] F. Wang, H. Zhai, Y. Ran, A. Vishwanath, and D.-H. Lee, Phys. Rev. Lett. 102, 047005 (2009); F. Wang, H. Zhai, D.-H. Lee, Europhys. Lett., **85**, 37005 (2009).
 - [8] A. V. Chubukov, D. Efremov, I. Eremin, Phys. Rev. B **78**, 134512 (2008).
 - [9] For a recent review of theoretical studies of the pairing mechanism in the iron based superconductors, see F. Wang and D.-H. Lee, Science **332**, 200 (2011).

- [10] W. L. McMillan, Phys. Rev. **167**, 331 (1968).
- [11] I. I. Mazin, D. J. Singh, M. D. Johannes, and M. H. Du, Phys. Rev. Lett. **101**, 057003 (2008)
- [12] I. I. Mazin, Phys. Rev. B **84**, 024529 (2011).
- [13] M. Khodas, A. V. Chubukov, arXiv:1202.5563.
- [14] Y. Yamada, and G. Shirane, J. Phys. Soc. Jpn. **26**, 396 (1969).
- [15] C. Husemann, and M. Salmhofer, Phys. Rev. B **79**, 195125 (2009).
- [16] Wan-Sheng Wang, Yuan-Yuan Xiang, Qiang-Hua Wang, Fa Wang, Fan Yang, and Dung-Hai Lee, Phys. Rev. B **85**, 035414 (2012).
- [17] F. Chen, *et al.*, Phys. Rev. X **1**, 021020 (2011).
- [18] D. J. Scalapino, J. R. Schrieffer, and J. W. Wilkins, Phys. Rev. **148**, 263 (1966).
- [19] J. L. M. van Mechelen, D. van der Marel, C. Grimaldi, A. B. Kuzmenko, N. P. Armitage, N. Reyren, H. Hagemann, and I. I. Mazin, Phys. Rev. Lett. **100**, 226403 (2008); J. L. M. van Mechelen *et al.*, Phys. Rev. Lett. **100**, 226403 (2008).
- [20] This issue has been raised in H. Kontani and S. Onari, Phys. Rev. Lett. **104**, 157001 (2010).
- [21] C. H. Perry, and T. F. McNelly, Phys. Rev. **154**, 456 (1967); C. H. Perry, R. Currat, H. Buhay, R. M. Migoni, W. G. Stirling, and J. D. Axe, Phys. Rev. B **39**, 8666 (1989).
- [22] Zhong-Yi Lu, private communication.
- [23] Yuan Wan and Qiang-Hua Wang, EPL **85**, 57007 (2009). In this paper symmetries of bilinears involving xz and yz orbitals are considered, but extension to five orbitals is straightforward.